Tunnel Heading Stability in Drained Ground

By Pieter A. Vermeer, Nico Ruse and Thomas Marcher

When considering ground conditions for tunnelling one might distinguish between ground with and without a macro structure due to stratification, schistosity and jointing. In this study attention is focused on soils and very soft rock without a significant macro structure. These materials tend to be encountered for shallow tunnelling in urban areas, whereas macro-structured ground is dominant in deep tunnelling. For soils and very soft rock, as considered in this study, stability is governed by shear strength parameters that can be measured in laboratory tests. For soft soils with little (effective) cohesion, it is necessary to drive the tunnel using a shield. For soils or rock with greater cohesion, it is possible to use an open face tunnelling method such as the NATM. Here, if necessary the stability of the tunnel face can be improved by inclining the face or by reducing the cross section of the excavation. In this study we will consider face stability both for closed-face shield tunnelling and open-face NATM tunnelling.

When discussing previous research on tunnel heading stability, one has to distinguish between drained and undrained conditions. For undrained conditions, as dominant in clays, practical design curves have been derived on the basis of model tests (2) and these curves have been largely confirmed by theoretical studies (8). The question whether a drained or undrained stability analysis should be carried out can be answered by considering the type of ground and the advance rate of the tunnel face. According to a parametric study by Anagnostou and Kovári (1), drained conditions tend to apply when the ground permeability is higher than 10^{-7} to 10^{-6} m/s and the net excavation advance rate is 0.1 to 1.0 m/hr or less. In a predominately sandy soil, therefore, drained stability conditions should be considered. In a clayey, low-permeability soil the undrained analysis is valid during excavation, but the drained analysis applies in case of a standstill. Hence, even for excavations in clay it is important to investigate drained soil conditions.

It would seem that Horn (25) was one of the first to propose a model for assessing the stability under drained conditions. He considered the limit equilibrium of a sliding wedge at the tunnel face. Jancsecz and Steiner (11) applied this model to shield-tunnelling, whilst Sternath and Baumann (19) used it to analyse NATM-tunnelling.

The idea of considering drained stability on the basis of a single equation was first suggested by Atkinson and Mair (2), as they proposed a formula

Standsicherheit der Ortsbrust von Tunneln unter dränierten Baugrundbedingungen

Die Standsicherheit der Ortsbrust von Tunneln wird zunächst im Hinblick auf Schildvortrieb betrachtet. Anschließend wird die Spritzbetonbauweise einbezogen, indem an der Ortsbrust von keinem Stützdruck ausgegangen wird. Mit der Absicht, einfache Formeln zu entwickeln, werden zunächst Tunnel mit einem Kreisquerschnitt in homogenem, dräniertem Mohr-Coulomb Material betrachtet. Ergebnisse aus nichtlinearen Finite-Elemente-Berechnungen werden verwendet, um zu zeigen, wie zumindest in Reibungsmaterial die Spannungsverteilung am Tunnel durch Gewölbewirkung dominiert wird. Wenn der Reibungswinkel größer als 20° ist, scheint die Standsicherheit der Ortsbrust völlig unabhängig von der Überdeckung des Tunnels zu sein. Unter dränierten Bedingungen scheint die Spritzbetonbauweise möglich zu sein, wenn die effektive Kohäsion etwa 10 % von γD erreicht, wobei γ die Bodenwichte ist. D ist entweder der Durchmesser des Tunnels bei einem Vollausbruch oder der Durchmesser der Ausbruchsfläche bei Teilausbruch. Bei der Betrachtung typischer Querschnitte von NÖT-Tunneln wird gezeigt, daß ein äquivalenter Wert für D in den Standsicherheitsformeln verwendet werden kann. In geschichtetem Baugrund sind die Gleichungen schwierig anzuwenden, weswegen dafür eine numerische φ-c-Reduktion vorgeschlagen wird.

Tunnel heading stability is initially considered with a view towards closed face tunnelling. At the end open face tunnelling is included by assuming face pressures to be equal to zero. In order to arrive at simple formulas, attention is initially focused on circular tunnels in a homogenous Mohr-Coulomb material. Data from non-linear finite element analyses are used to show that stress distributions in drained ground are dominated by arching. Once the friction angle is larger than about 20°, stability appears to be completely independent of the cover on top of the tunnel. For drained conditions, open face tunnelling appears to be possible when the effective cohesion exceeds some 10 % of $\gamma \cdot D$, where γ is the unit soil weight. Here D may either be the full tunnel diameter or a subsection diameter of a sequential excavation. Considering typical shapes of NATM tunnels, it is shown that an equivalent D-value can be calculated for use in the stability formulas. For layered ground, the formulas are difficult to apply and it is proposed to use a numerical procedure named φ-c-reduction method.

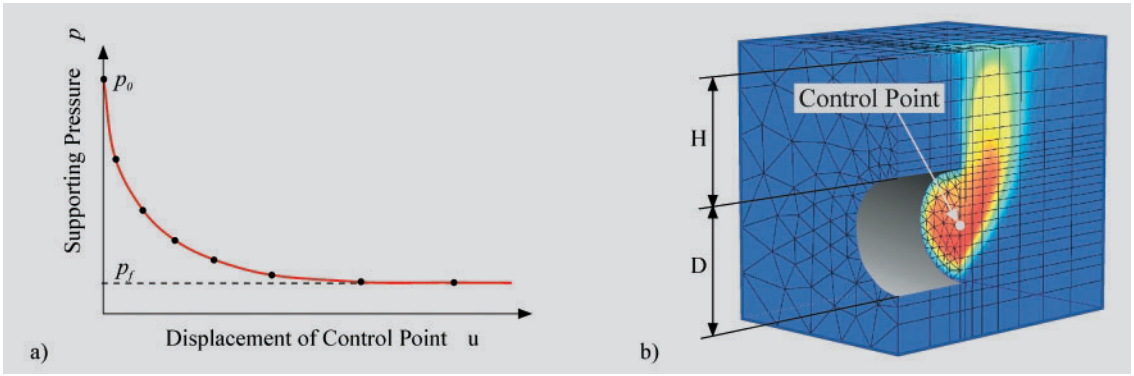

Fig. 1 Typical pressure-displacement curve (a) and flow area at collapse (b).

Bild 1 *Typische Druck-Verschiebungskurve (a) und der Fließbereich im Bruchzustand (b).*

of the form $p_f = qN_q + \gamma DN_\gamma$ for shield tunnels in dry cohesionless sand. Here p_f is the minimum support pressure at collapse, which will be referred to as failure pressure. The influence of a possible ground surface load is taken into account by a uniformly distributed load q and a surcharge stability number N_q. The diameter of the tunnel is denoted as D, the unit soil weight as γ and N_γ is the soil weight stability number. It should be noted that Atkinson and Mair used the symbol T to denote stability numbers. The above formula for failure pressure was extended by Anagnostou and Kovári (1) to cover cohesive-frictional materials by proposing an equation of the form

$$p_f = -c'N_c + qN_q + \gamma DN_\gamma \quad \text{.....[1]}$$

where c´ is the effective cohesion and N_c the cohesion stability number. Anagnostou and Kovári denoted stability numbers by the symbol F instead of N. The stability numbers are analogous to the bearing capacity factors of footings, in the sense that they depend on the friction angle j´. Vermeer and Ruse (20) presented data from elastic-plastic finite element analyses to show that the stability numbers are independent of the depth of the tunnel, at least for friction angles beyond twenty degrees. Moreover, simple formulas were put forward for the stability numbers. Later Vermeer and Ruse (21) extended this study by considering non-circular cross-sections to show that the shape of the excavation is not particular important.

The present paper summarises first of all previous research on stability numbers for drained situations. Hereafter the influence of an unlined wall near the tunnel face is considered, and attention is focused on NATM tunnelling without any supporting pressure. This paper will concentrate mainly on results from numerical simulations, and for this reason a brief description of the finite element procedure being used will be given in the following section.

Finite element-analyses of failure pressures

Semprich (18) was one of the first to perform three-dimensional finite element calculations to analyse the deformations near an open tunnel face. More recently Baumann et al. (3) studied the face stability of tunnels in soils and soft rocks by using the finite element method in combination with the elastic-plastic Mohr-Coulomb constitutive model. Several authors (22, 24) have shown that the elastic-plastic finite-element method is well-suited to predict collapse loads of geotechnical structures. For limit load analyses, pre-failure deformations are not of great importance and are assumed to be linearly elastic, as is usual within the elastic-plastic Mohr-Coulomb model being used in this paper. Elastic strains are governed by the elasticity modulus E and Poisson´s ratio v. The particular values of these input parameters influence load-displacement curves as shown in Figure 1a, but not the failure pressure p_f. For this reason they will not get any further attention in this study. In addition to the elasticity modulus and Poisson´s ratio, there are three material parameters for the plastic behaviour: the effective cohesion c´, the effective angle of friction φ' and the angle of dilatancy ψ. Different dilatancy angles give different load-displacement curves and different collapse mechanisms, but they have very little influence on the failure load. For this reason, nearly all our computations were performed for non-dilatant material.

As symmetrical tunnels are considered, the collapse-load calculations are based on only half a circular tunnel which is cut lengthwise along the central axis. Figure 1b shows a typical finite element mesh as used for the calculations. The ground is represented by 15-noded prismatic volume elements and the tunnel lining is modelled with 8-noded shell elements. The boundary conditions of the finite element mesh are as follows: The ground surface is free to displace, the side surfaces have roller boundaries and the base is fixed. It is assumed that the distribution of the initial stresses is geostatic according to the rule $\sigma'_h = K_0 \sigma'_v$, where σ'_h is the horizontal effective stress and σ'_v is the vertical effective stress. K_0 is the coefficient of lateral earth pressure. Vermeer and Ruse (20) investigated the possible influence of the initial state of stress, by varying the coefficient of lateral earth pressure and found that the K_0-value influences the magnitude of the displacements but not the pressure at failure.

The first stage of the calculations is to remove the volume elements inside the tunnel and to activate the shell elements of the lining. This does not disturb the equilibrium as equivalent pres-

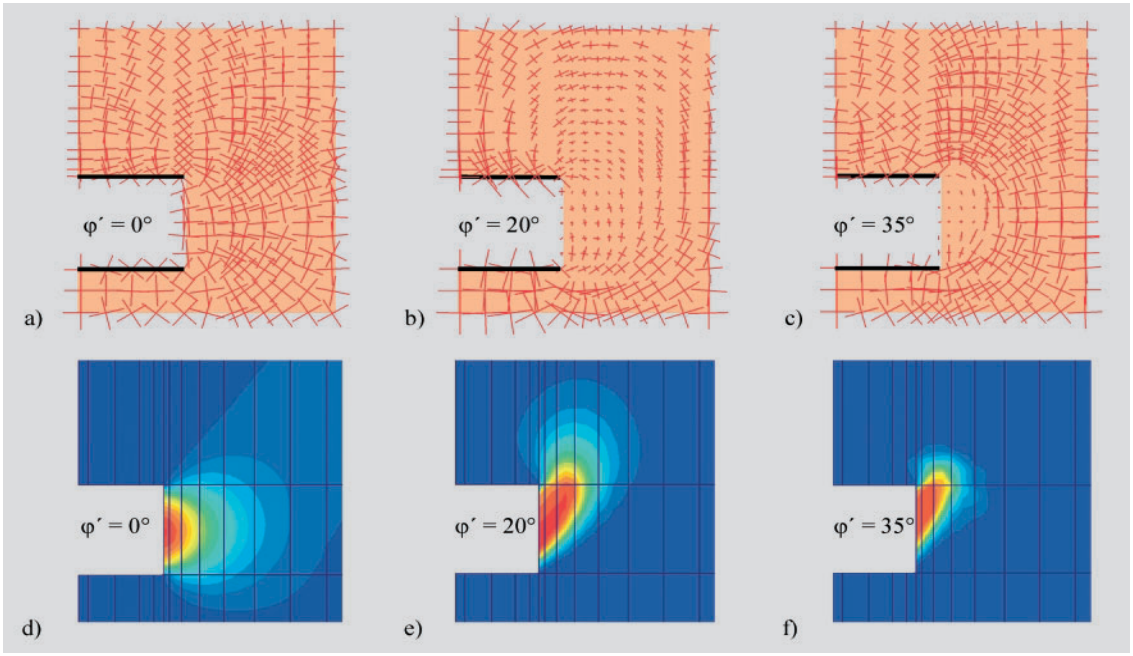

Fig. 2 Principal stresses (a - c) and incremental displacements (d - f) at failure. Close-up around the face for a tunnel with H/D = 5.

Bild 2 *Hauptspannungen (a - c) und inkrementelle Verschiebungen (d - f) im Bruchzustand. Ausschnitt aus dem Bereich der Ortsbrust für einen Tunnel mit H/D = 5.*

sures are applied on the inside of the entire tunnel. To get a full equivalence between the initial supporting pressure and the initial geostatic stress field, the pressure distribution is not constant but increases with depth. This is obviously significant for very shallow tunnels, but a nearly constant pressure occurs for deep tunnels. The minimum amount of pressure needed to support the tunnel is then determined by a stepwise reduction of the supporting pressure.

A typical pressure-displacement curve is shown in Figure 1a, where p is the supporting pressure at the level of the tunnel axis and u the displacement of the corresponding control point at the tunnel face. The control point has to be chosen within the collapsing body; otherwise the load-displacement curve in Figure 1a will come to an almost sudden end and the curve then cannot be used to conclude that failure has been reached. Rather than selecting a single control point, it is appropriate to select a few of such points. With the reduction in supporting pressure, there is increasing displacement. When failure occurs the curve has become horizontal. For shallow tunnels, a chimney-like collapse mechanism is obtained as indicated in Figure 1b, where incremental displacements at failure are shown as graded shades from blue to red.

Upon extending finite element procedures to limit load computations, it appears that the entire numerical procedure should be well designed in order that an accurate assessment of the failure load can be made. For each decrement of supporting pressure, equilibrium iterations are performed and plastic stress redistribution is accomplished by using a radial-return algorithm. A general validation of the computer code is given in the manual of the 3D-Plaxis program by Brinkgreve and Vermeer (4) and the method of collapse load computations is fully described by Vermeer and Van Langen (22). In more recent papers the authors have shown that such finite element analyses can also yield highly accurate data on failure pressure of tunnel headings.

Arching at the face of fully lined tunnels

Besides failure pressures, the finite element-method produces insight into the stress distribution around a tunnel face and the role of friction. This can be seen from Figure 2 for a tunnel with a relative ground cover of H/D = 5. In this figure principal stresses are plotted in lengthwise sections through circular tunnels; firstly for a tunnel in non-frictional soil, secondly for a friction angle of only 20° and finally for a highly frictional material with a friction angle of 35°. In all these different cases the ground is non-cohesive and the supporting pressure has been reduced down to the failure pressure by performing three-dimensional finite-element analyses. Moreover, fully lined tunnels are considered with a lining up to the very tunnel face.

Figure 2a shows a stress distribution with stress crosses that rotate around the tunnel face. All these crosses have about the same size, which indicates a high supporting pressure. On the other hand, small stress crosses are seen around the tunnel face of Figure 2b. Hence in frictional material the failure pressure is relatively low. For the highly frictional material of Figure 2c, the arching is extremely clear. Here the supporting pressure is nearly equal to zero and a strong stress arch is observed directly between the top and the bottom of the tunnel.

The influence of the angle of friction can also be recognised by the failure patterns in Figures 2d to 2f. Here increasing displacements at failure are shown in graded shades from blue to red. One observes in Figure 2d the extreme of a non-frictional material that flows more or less like a liquid into the tunnel. For a moderate friction angle of

20°, one observes in Figure 2e the development of a tall cave. In case of a shallow tunnel this type of failure will extend to the surface to create a crater. For the highly frictional soil of Figure 2f, a relatively small body is dropping into the tunnel.

The consequences of friction dependent arching are considerable. The stress arch carries the ground cover independent of the magnitude of its thickness. In an earlier study by Vermeer and Ruse (20) the ground cover has been varied systematically to assess its influence on the failure pressure. It appeared that once the friction angle is larger than about twenty degrees, stability is completely independent of the ground cover. Considering non-cohesive ground, it was found from a series of 25 different calculations that $p_f = \gamma D N_\gamma$ with

$$N_\gamma = \frac{1}{9 \tan \varphi'} - 0.05 \quad \text{.....[2]}$$

under the conditions that $\varphi' > 20°$ and $H/D > 1$. Hence, the soil weight stability number is dependent on friction, but not dependent on ground cover.

Figure 3 shows that the finite element method (FEM) yields soil-weight stability numbers between the theoretical bound solution by Léca and Dormieux (14) and the results of a study by Krause (13). The latter assumed a shell-shaped failure body at the tunnel face that can slide into the tunnel. In finite element analyses no assumption at all is made about the failure mechanism and both dome-like failure bodies are found, as observed in Figure 2e, and shell-shaped ones (see Figure 2d) can be obtained. Anagnostou and Kovári (1) present curves for N_γ which lie well above the FE-results. Their sliding wedge model yields slightly different curves for different relative depths. The lower boundary of the shaded area in Figure 3 corresponds to $H/D = 1$ and the upper one to situations with $H/D > 5$. Hence, the sliding wedge model would seem to be very conservative when cohesionless soils with friction angles less than about 30° are considered. The curve by Atkinson and Mair (2) is extremely conservative as it is based on 2D-experiments, that show obviously less arching as 3D tunnel headings.

For high friction angles above forty degrees, most existing models give $N_\gamma \approx 0.1$ and match the experimental data by Chambon and Corté (6) reasonably well, as can be seen in Figure 3. The experimental data were obtained from 3D centrifuge tests with nearly cohesionless sand and friction angles in the range between 38° and 42°. All their experimental data, i.e. assuming $c' = 0$ as well as $c' = 2.5$ kPa, fit into the shaded bar in Figure 3.

The stability numbers for cohesion and surcharge

In contrast to the soil weight number, the cohesion number can be derived theoretically. In fact, Vermeer and Ruse (20) derived the simple expression $N_c = \cot \varphi'$, which was also verified by use of the finite element method (FEM). Again this expression can be compared to findings by other researchers, as also done in Figure 4. Once more Krause´s results (13) are based on a shell-shaped failure body, whereas the data by Anagnostou and Kovári (1) are based on the sliding wedge model, as also described by Jancsecz and Steiner (11).

The theoretical derivation of $N_c = \cot \varphi'$ is based on the assumption that ground surface loads have no influence at all. In other words the stability number N_q in equation [1] is supposed to be equal to zero. This has been checked by performing a series of 24 finite element analyses with different uniformly distributed surface loads q and resulting data are presented in Figure 5. For friction angles above 25°, it is observed that a surface load has no influence on the failure pressure. In these cases arching is apparently so strong that all surface loads can be carried, independent of the ground cover on top of the tunnel. For a low friction angle of only 20°, however, the situation is slightly different. In this case

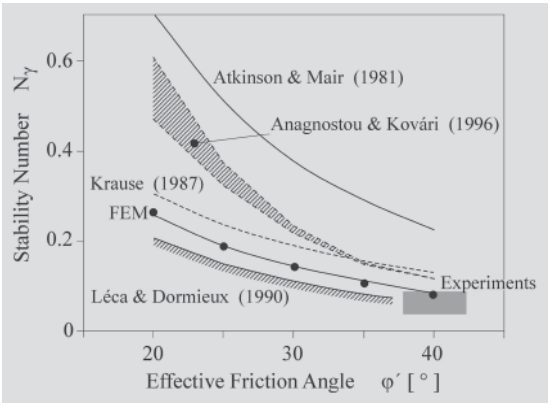

Fig. 3 The soil weight stability number as determined by different methods.

Bild 3 *Die Stabilitätszahl N_γ für vollständig ausgekleidete Tunnels nach verschiedenen Methoden.*

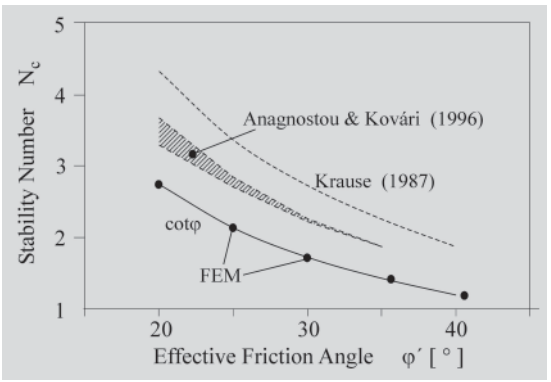

Fig. 4 The cohesion stability number according to different models.

Bild 4 *Der Kohäsionsbeiwert N_c auf der Grundlage verschiedener Modelle.*

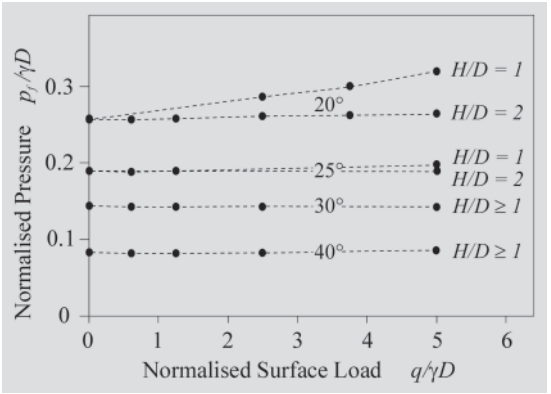

Fig. 5 Influence of uniformly distributed surface load on failure pressure.

Bild 5 *Einfluß einer gleichmäßig verteilten Auflast an der Geländeoberfläche auf den Bruchdruck.*

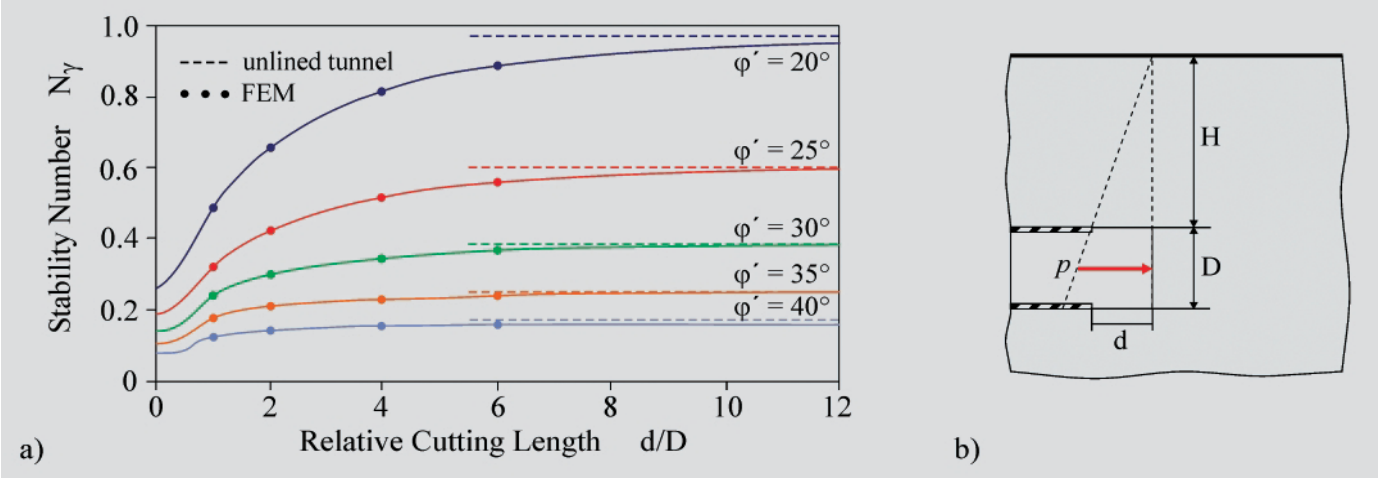

Fig. 6 The soil weight stability number as a function of the relative cutting length.

Bild 6 *Die Stabilitätszahl N_γ als Funktion der relativen Abschlagslänge.*

one needs a ground cover of at least twice the tunnel diameter to eliminate the influence of a surface load completely. For a friction angle of 20° and a cover of H = D, on the other hand, one observes a small increase of the failure pressure as a function of q such that $N_q \approx 0.01$. Compared to the soil weight stability number of about 0.25 (see Figure 3 for φ´ = 20°) and the cohesion stability number of 2.75 (see Figure 4), a N_q-value of 0.01 is very low and it can be disregarded. Hence

$$N_q \approx 0 \quad \text{and} \quad N_c = \cot \varphi' \qquad [3]$$

at least under the conditions that φ´ > 20° and H > 2D. This relatively large cover is, however, not needed for high friction angles. For friction angles beyond 25° the above equation appears to hold for smaller values of H, namely for H > D.

Influence of an unlined wall near the tunnel face

In order to determine the influence of an unlined wall with length d near the tunnel face, as indicated in Figure 6b, additional finite element analyses were carried out. In these analyses a supporting pressure was applied both at the tunnel face and at the unlined part of the wall. This supporting pressure was then reduced until failure occurred.

Fig. 7 The soil weight stability number as a function of the relative cutting length.

Bild 7 *Die Stabilitätszahl N_γ als Funktion der relativen Abschlagslänge.*

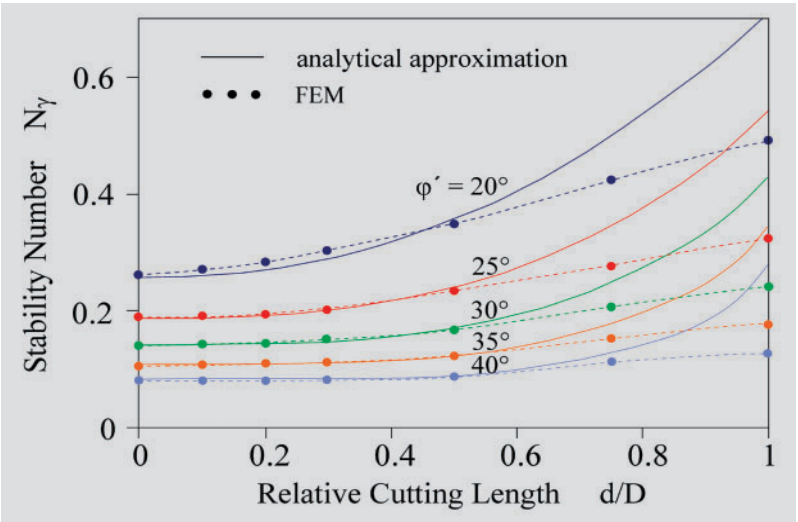

Again circular tunnels are considered and again we begin to consider purely frictional soil without any effective cohesion. Then it was found from a series of 75 different calculations that $p_f = \gamma D N_\gamma$ with the stability numbers as plotted in Figure 6. It shows that the soil weight stability number increases as a function of the relative cutting length d/D. Different curves are obtained for different friction angles, but all curves show basically the same shape. Indeed, up to d = D the curves are concave and then one observes a convex shape. Finally they approach an asymptotic limiting value that depends on the friction angle. The asymptotic values correspond to completely unlined tunnels.

Considering the complex shape of the curves in Figure 6a, it would seem difficult to find an analytical expression that matches these curves. For small values of d/D, however, the curves have a simple concave shape, and the following fairly simple analytical approximation can be used:

$$N_\gamma = \frac{2 + 3\,(d/D)^{6 \tan \varphi'}}{18 \tan \varphi'} - 0.05 \qquad [4]$$

under the conditions that φ´ > 20° and d < 0.5D. This analytical approximation reduces to equation [2] when the cutting length is equal to zero. It matches the computational results up to d = 0.5D, as can be seen in Figure 7 that shows a close up of Figure 6a. It is expected that equation [4] is valid for a ground cover of at least 1.5D, but as yet this has not been investigated. On considering Figure 7, it would seem that the cutting length has relatively little influence on the tunnel heading stability. In particular up to d/D = 0.3, the soil weight stability number is found to be nearly independent of the cutting length.

The relatively small influence of the cutting length would seem to suggest that safety can hardly be improved by a reduction of the cutting length, but distinction should be made between drained and undrained conditions. Indeed, all results apply to drained situations with considerable arching and consequently a relatively small influence of the cutting length. For undrained conditions, on the other hand, the situation is different. Here model test results on tunnels in clay by Kimura and Mair

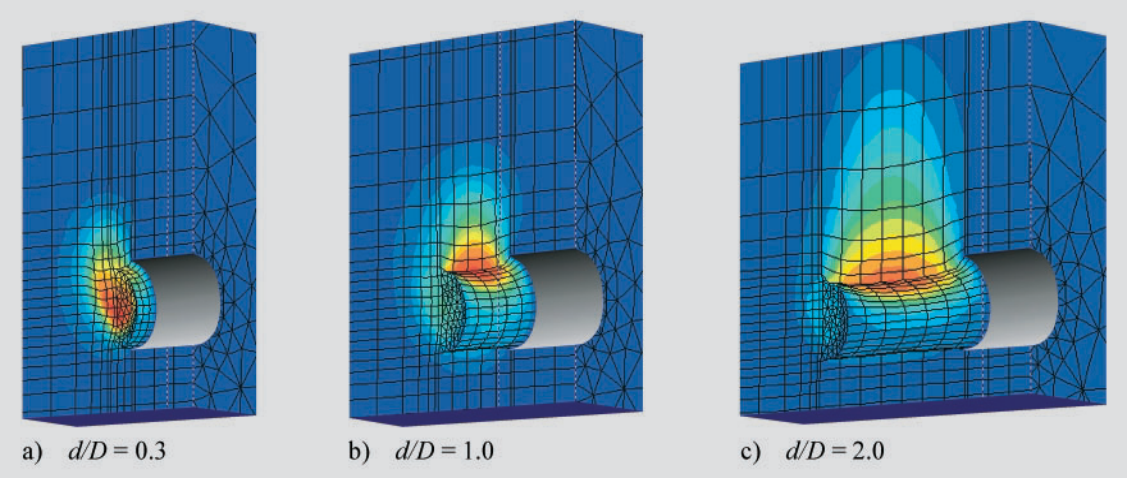

Fig. 8 Incremental displacements at failure for different cutting lengths. Red colour indicates the zone with the largest incremental displacements.

Bild 8 *Inkrementelle Verschiebungen im Bruchzustand bei unterschiedlichen Abschlagslängen. Rot gibt die Bereiche mit den größten inkrementellen Verschiebungen an.*

(12) have shown a clear influence of the cutting length. This was even observed for small lengths where drained analyses show little or no influence of d. It should also be realised that our "drained" formulas have been derived for circular tunnels in non-layered ground. In a later section it will be shown that the influence of the cutting length is somewhat more important when considering NATM-shapes. Finally a significant influence of the cutting length will be reported later, when considering NATM tunnels in layered ground.

Having shown failure mechanisms for fully lined tunnels in Figure 2, it is now of interest to consider collapse patterns for partially lined tunnels. To this end computational data are shown in the three-dimensional perspective in Figure 8. It shows close ups around the heading of deep tunnels with different cutting lengths in ground with a friction angle of 30°. The lining is indicated by shades from white to black, the volume elements of the ground by black lines. Similar to Figures 2e to 2f the rate of displacements are shown in graded shades from blue to red. For small values of d, the failure mechanism remains at the tunnel face (Figure 8a), but for larger values one observes a collapsing roof (Figures 8b and 8c).

Fully unlined tunnels

On increasing the cutting length up to extremely large values, one finally obtains the two-dimensional situation of an unlined tunnel. The data in Figure 6 indicate that such a situation is virtually reached when $d > 10D$. Vermeer and Vogler (2002) performed two-dimensional analyses of unlined tunnels and reported for the soil weight stability number the expression

$$N_\gamma = 0.6\cot^2 2\varphi' + 0.18 \qquad \text{for } d = \infty \quad \ldots\ldots\ldots\ldots [5]$$

under the conditions that $\varphi' > 25°$ and $H/D > 2$. On comparing the extremes of a fully lined tunnel with $d = 0$ (equation [2]) and a fully unlined one with $d = \infty$ (equation [5]), one compares a face failure as indicated in Figure 8a with a plane strain roof failure. The difference is tremendous and this is also reflected in the failure pressure; Figure 6a shows that failure pressures differ at least a factor two and for low friction angles even more than a factor three. This demonstrates that the three-dimensional arching for $d = 0$ is much stronger than the two-dimensional arching for $d = \infty$. The data by Vermeer and Vogler (23) also show that full two-dimensional arching, such that the failure pressure is independent of depth, requires a relatively large friction angle of at least 25° and a relatively large ground cover of at least 2D.

As the unlined tunnel involves a roof failure, it is logical to plot the supporting pressure as a function of the roof settlements. In this case the curve of Figure 1a reduces to the well-known ground response curve (15), which plays an important conceptual role in NATM tunnelling. In addition there is the idea of a supporting ground ring as indicated in Figure 9a. We will consider a

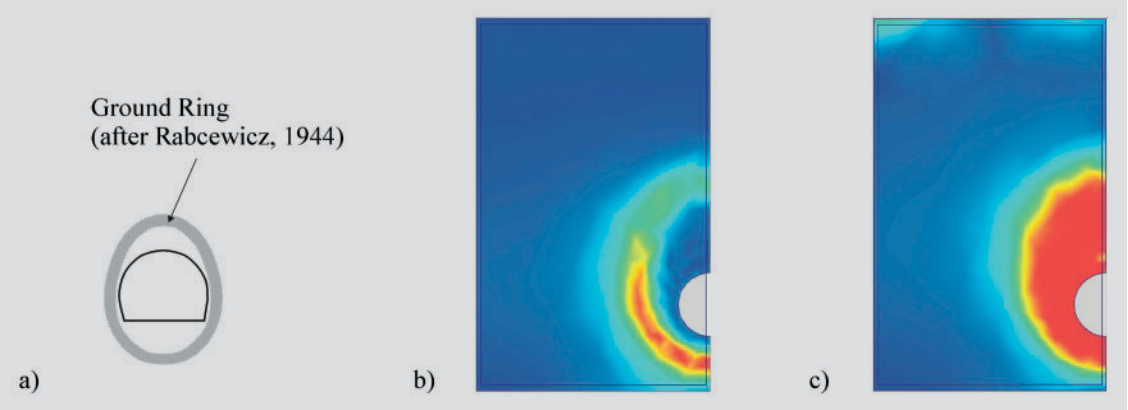

Fig. 9 a) The idea of a ground ring, b) deviatoric stresses $|\sigma_1 - \sigma_3|$, c) mobilised shear strength for a deep tunnel.

Bild 9 *a) Die Idee des Gebirgstragrings, b) Deviatorspannungen $|\sigma_1 - \sigma_3|$, c) mobilisierte Scherfestigkeit für einen tiefen Tunnel.*

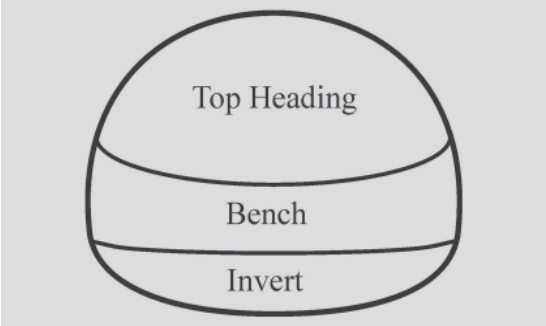

Fig. 10 Possible sequential excavations.
Bild 10 *Mögliche Teilausbruchsflächen.*

cross-section around a tunnel in order to investigate whether or not a so-called pressure ring in the sense of Rabcewicz (17) will be formed. Within such a ring one would expect tangential normal stresses (σ_1) that are large with respect to the radial normal stresses (σ_3). The stress difference σ_1-σ_3 has thus been visualised to obtain Figure 9b.

The red colour in Figure 9b is used to indicate extreme stress differences and the blue colour means that there is either an isotropic state of stress with $\sigma_1 = \sigma_3$ or a state with very low stresses. The large blue zone in Figure 9b relates to the assumption of an initial isotropic state with $\sigma_1 = \sigma_3$. The smaller blue area just around the tunnel indicates a zone with very small stresses. The red-green oval around the tunnel indicates an arching ground ring in the sense of Rabcewicz (17). The ring is characterised by large tangential stresses (σ_1) and small radial stresses (σ_3). Excentric ovals around the tunnel can also be observed in Figure 9c. This figure shows the mobilisation of the shear strength $\tau_f = c' + \sigma' \tan \varphi'$. The red colour indicates full mobilisation and the blue colour is used for the area where there is no mobilisation at all, i.e. a zone with $\sigma_1 = \sigma_3$. This study thus confirms the idea of a pressure ring around a tunnel. It is particularly observed when considering principal stress differences, as done in Figure 9b.

Maximum diameter in open-face tunnelling

In usual open-face tunnelling, the face pressure is equal to zero and the failure pressure as computed from equation [1] must be negative; otherwise the situation would not be stable. Open-face tunnelling is thus subject to the criterion $p_f < 0$. In order to consider this criterion in more detail, expressions [3] and [4] for the stability numbers are substituted into equation [1] to obtain:

$$p_f = \gamma D \left(\frac{2 + 3(d/D)^{6 \tan \varphi'}}{18 \tan \varphi'} - 0.05 \right) - \frac{c'}{\tan \varphi'} \quad \text{.....[6]}$$

under the conditions that $\varphi' > 20°$ and $d/D < 0.5$. The stability criterion $p_f < 0$ can now be reformulated to obtain an upper bound for the diameter of a tunnel. It yields for $d/D < 0.5$

$$D \leq \frac{18 c'/\gamma}{2 + 3(d/D)^{6 \tan \varphi'} - 0.9 \tan \varphi'} \quad \text{.....[7]}$$

This equation would seem to be implicit in terms of the diameter, but this is not the case as long as d/D has a given constant value. On the other hand, if the cutting length is taken as a constant rather than the relative cutting length d/D, one has to solve the above equation iteratively. In many practical situations, however, d/D is relatively small and its contribution to equation [7] can be disregarded. On disregarding this term one obtains for $d/D < 0.3$

$$D \leq \frac{9c'}{\gamma} \frac{1}{1 - 0.45 \tan \varphi'} \quad \text{.....[8]}$$

It can be observed from this equation that the angle of friction makes only a moderate contribution to the safety of an open tunnel face. One can consider for example a soil with a friction angle of only 20°, then equation [8] yields $\gamma D < 10\ c'$. For a friction angle of 30°, the situation is only slightly better as equation [8] then gives $\gamma D < 12\ c'$. Hence the friction angle is not of great importance. It can thus be concluded that open face tunnelling under drained conditions is possible when the effective cohesion is at least 10 % of γD.

If the cohesion is large enough a tunnel can be driven at its full size. In case of relatively small values of c′, on the other hand, the tunnel can be driven in sections (Figure 10). In the latter case of a sequential excavation the equivalent diameter of the top heading applies and equation [8] can be used to compute its maximum value. The above condition [8] on the tunnel diameter demonstrates the impact of the cohesion in open-face tunnelling. The maximum diameter is simply linearly related to the cohesion.

Factor of safety for open-face tunnelling

Instead of computing a maximum tunnel diameter, as done in the previous section, it is possible to consider a tunnel with a given diameter and to compute a factor of safety. In structural engineering the safety factor is usually defined as the ratio of the collapse load to the working load, but for tunnel headings, this definition is not appropri-

Fig. 11 An entrance of the Rennsteig tunnel.
Bild 11 *Portalbereich des Rennsteigtunnels.*

ate. Here one better adopts the definition that is used in the analysis of slope stability, i.e.

$$\eta = \tau_f / \tau_{mob} \quad \text{.....[9]}$$

where τ_f represents the shear strength. This ratio of the shear strength to the mobilised strength is a safety factor, which is to be considered in the rest of this paper. By introducing the definition $\tau_f = c' + \sigma' \tan \varphi'$, where σ' is the effective normal stress on a potential slip plane, the safety factor is found to be

$$\eta = \frac{c' + \sigma' \tan \varphi'}{c_{mob} + \sigma' \tan \varphi_{mob}} \quad \text{.....[10]}$$

The parameters c_{mob} and φ_{mob} are mobilised shear strength parameters that are just large enough to maintain equilibrium. Let us now return to equation [6], where the failure pressure p_f is related to the shear strength parameters. This relationship does not only hold for the parameters p_f, c' and φ' but also for the mobilised ones p_{mob}, c_{mob} and φ_{mob}. It yields

$$p_{mob} = \gamma D \left(\frac{2 + 3(d/D)^{6 \tan \varphi_{mob}}}{18 \tan \varphi_{mob}} - 0.05 \right) - \frac{c_{mob}}{\tan \varphi_{mob}} \quad \text{.....[11]}$$

where p_{mob} is the really applied face pressure. Within the concept of a single global factor of safety it is appropriate to define $c_{mob} = c'/\eta$ and $\varphi_{mob} = \varphi'/\eta$, as also suggested by equation [10]. On substituting these expressions into equation [11] and on considering open-face tunnelling with $p_{mob} = 0$, it follows that

$$\eta = \frac{0.9 \tan \varphi' + 18 c'/\gamma D}{2 + 3(d/D)^{6 \tan \varphi'/\eta}} \quad \text{.....[12]}$$

For d = 0 the safety factor can be computed straight forwardly, but an iterative procedure is needed when the cutting length is not equal to zero. However, the influence of the cutting length on the safety factor is relatively small, as already discussed in a section above. For usual friction angles beyond 20° and safety factors below $\eta = 1.5$, it can be shown that

$$0.87 \eta_{d=0} < \eta \leq \eta_{d=0} \quad \text{for } d < 0.2D \text{ .....[13]}$$

Hence, the influence of the relative cutting length on the safety factor is below 13 % and a relatively close estimate of the safety factor is thus obtained on using d = 0. For a more exact solution of equation [12], the factor $\eta_{d=0}$ can be used as a first iterate and a nearly exact solution will be found when performing two or three iterations.

Up to now open-face tunnelling has been considered to be a special case of closed-face tunnelling, i.e. by setting p_{mob} equal to zero. In non-linear finite element analysis, however, the factor of safety can be computed directly by means of so-called φ-c-reduction. This procedure was basically proposed by Zienkiewicz (24), improved by Brinkgreve and Bakker (4) and also published by

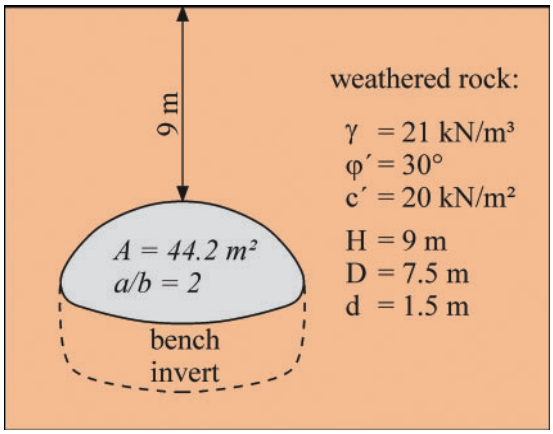

Fig. 12 Top heading of Rennsteig tunnel in homogeneous ground.
Bild 12 *Kalottenvortrieb des Rennsteigtunnels in homogenem Baugrund.*

Dawson et al. (9). The procedure has been implemented in the Plaxis code (5) as well as in the FLAC code (10). In this φ-c-reduction procedure the actual shear strength parameters are proportionally reduced until failure occurs for c_{mob} and φ_{mob}. Then the factor of safety is obtained from the ratio of c' and c_{mob}, or equivalently from the ratio of $\tan \varphi'$ and $\tan \varphi_{mob}$. Several such calculations where performed by Vermeer and Ruse (21) in order to validate equation [12] for circular tunnels in homogeneous ground.

NATM-tunnel in homogeneous ground

As a first case study a cross section of the Rennsteig tunnel in Thuringia is considered. This relatively new tunnel with a length of nearly 8 km is part of the German motorway A71 (Figure 11). The excavation of the double-tube tunnel was done by a sequential construction of a top heading followed by bench and invert. Figure 12 shows a particular cross section with a relatively small ground cover of only 9 m. We have analysed this cross section both for uniform ground as well as for a layered ground profile. The layered ground profile is to be considered in a subsequent section. In this section a non-layered ground with properties as indicated in Figure 13 is to be considered.

Attention will be focused on the stability of the non-circular top heading. Here it might be wondered whether or not such an oval shape can be considered on the basis of equation [12], as this relation was derived for circular cross sections. However, it will be shown that equation [12] can handle non-circular NATM tunnels. In order to apply this equation, an equivalent tunnel diameter is needed. The top heading of the Rennsteig tunnel has a width of a = 11.5 m, a height of b = 5.3 m and a cross sectional area of 44 m². The area can be used to calculate an equivalent diameter of D = 7.5 m. The problem is now fully characterised by the parameter set in Figure 12. On using equation [12] this leads to a safety factor of $\eta = 1.36$.

In order to check the above result of equation [12], a finite element analysis has been carried out for the real non-circular cross section. In this numerical analysis both c' and φ' were step-

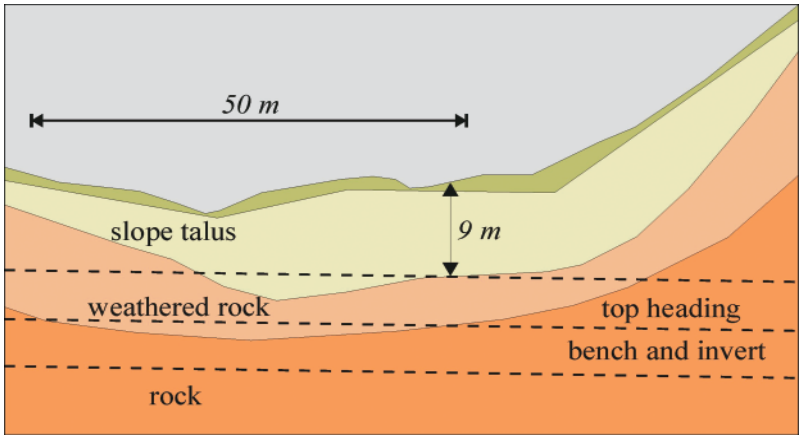

Fig. 13 Geological cross section of the Baecker Stream Valley.

Bild 13 *Geologischer Schnitt im Bereich Bäckerbachtal.*

wise decreased down to failure values, i.e. down to c_{mob} and φ_{mob}, as explained at the end of the previous section. In this manner a safety factor of $\eta = 1.35$ was obtained, being practically equal to the one from equation [12].

The considered cross section of the Rennsteig tunnel suffers from a relatively small ground cover of H/D = 1.2, where D is the equivalent diameter. In such a case one might wonder whether or not the stability of the tunnel heading is influenced by this small cover and for this reason we also analysed a situation with an extremely large ground cover. Again a factor of safety of about $\eta = 1.35$ was found, as also listed in the Table. This equivalence between the very shallow and the very deep tunnel may be more generally expected for friction angles above 25°. For lower angles of friction between 20° and 25°, depth independence requires relative ground covers of at least two, as also concluded from the data in Figure 5.

The nearly exact correspondence between present results for a circular shape and a top heading shape for d = 1.5 m are a coincidence. On using for instance d = 0 instead of d = 1.5 m, differences between both shapes are found to be larger. For zero cutting length, the top heading shape happens to yield $\eta = 1.48$, whereas a circular shape leads to $\eta = 1.40$ as listed in the Table. Hence, it would seem that the top heading shape tends to a slightly larger safety factor than the circular shape, but differences remain within a margin of 6 %. It is thus conducted that equation [12] applies both to circular shapes and NATM shapes.

NATM-tunnel in layered ground

Instead of considering tunnel excavations in homogeneous ground, as done in the previous section, attention will now be paid to excavations in layered ground. Again the top heading excavation of the Rennsteig tunnel is considered and the crossing of a valley with ground layers as indicated in Figure 13. On the extreme left hand side one observes that the top heading and the ground cover are nearly completely in a weathered rock layer. This case has already been considered in the previous section on non-layered ground. On moving from the left hand side of Figure 13 towards the middle, the ground cover changes from weathered rock into slope talus. The subsequent cross sections are clearly shown in Figure 14. Please note that the slope talus has a slightly smaller friction angle and a considerably smaller cohesion than the weathered rock underneath. The data for the weathered rock are as indicated in Figure 12 and the properties of the slope talus are indicated in Figure 14.

All three different cases in Figure 14 have been analysed numerically. As equation [12] does not hold for layered ground, safety factors were computed by performing three-dimensional finite element analyses. In all analyses the shape of the top heading was exactly modelled and the φ-c-reduction procedure was applied. The computed η-values are indicated in Figure 14 and show a very logical trend; the thicker the soft top layer, the lower the factor of safety. On plotting results as a function of the effective ground cover

$$H' = H - H_{\text{top layer}} \quad \text{.....[14]}$$

one obtains Figure 15, in which the safety factor is plotted as a function of the effective ground cover. This figure illustrates the impact of an effective ground cover. For relatively small effective ground covers, the safety factor depends significantly on this cover, but starting from $H' \approx D$, a more or less constant factor of safety is found. This is fully in the line with the data in Figure 5 on the influence of the ground cover. It is also fully in line with our findings of arching around tunnel headings. For $H' > D$ arching can fully develop and equation [12] applies. For smaller thicknesses of the effective cover, the soft layer plays a role and equation [12] should not be applied. Instead it is recommended to perform finite element analyses with φ-c-reduction, as done to obtain Figure 15. On decreasing H′ below the critical value of D, one observes first a gradual decrease of the safety factor and a dramatic decrease as soon as H′ has become negative.

For negative values of the effective ground cover, the tunnel face consists partly out of relatively soft ground and it influences the failure mechanism considerably. As long as the tunnel face is completely in the weathered rock, a full face failure is obtained, as indicated in Figures 2e and 2f. For the case of Figure 14c, on the other hand, a more local failure entirely inside the soft top layer was observed. Figure 16 shows the local failure for a situation with zero cutting length; on the left a cross section and on the right a longitudinal section of the top heading. Increasing displacements are shown in graded shades from blue to red.

Safety factors for Rennsteig tunnel in homogeneous ground.
Sicherheitsfaktoren für den Rennsteigtunnel in homogenem Baugrund.

Method	Geometry	$\eta_{d=0}$	$\eta_{d=1.5}$
Equation 12	circle	1.40	1.36
FEM	shallow top heading	1.48	1.35
FEM	deep top heading		1.37

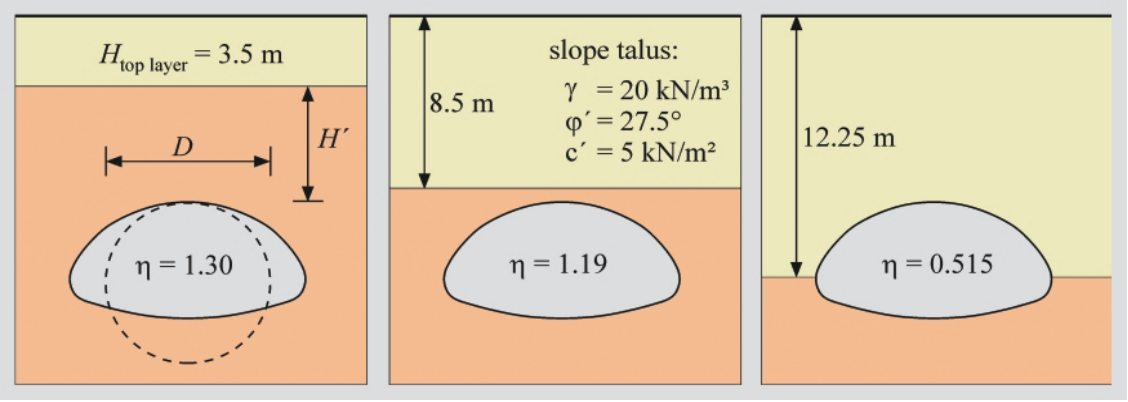

Fig. 14 Different ground profiles for Rennsteig tunnel with computed safety factors for d = 1.5 m.

Bild 14 *Verschiedene Bodenprofile für den Rennsteigtunnel mit den jeweils berechneten Sicherheitsfaktoren für d = 1,5 m.*

Let us now consider the influence of the cutting length in somewhat more detail. To this end, it should be realised that the very local face failure in Figure 16 corresponds to d = 0. For non-zero cutting lengths, however, the failure zone is larger due to the inclusion of the unsupported part of the tunnel roof. As long as the soft top layer is not far below the tunnel roof and significant cutting lengths are used, the failure mode is even a roof failure instead of a face failure. As a consequence of such different failure modes, the cutting length plays an important role in layered ground and this is reflected by the two curves in Figure 15.

On performing non-linear finite element analyses in layered ground, it appears that the element mesh should be well designed in order that an accurate assessment of the failure mechanism can be made. For meshes with 15-noded prismatic elements as illustrated in Figure 1b and homogeneous ground, fine meshes with an average element length of D/10 around the tunnel face were used. In order to obtain accurate results for tunnel faces in layered ground, refined meshes in the soft zones near the tunnel face were used, as failure tends to localise in such zones.

Conclusions

Results of three-dimensional finite element calculations have been considered for tunnel headings in drained ground. Restriction has been made to an isotropic Mohr-Coulomb material, which excludes materials with a highly anisotropic strength such as jointed rocks and heavily bedded sediments. Stress distributions around tunnel headings in soils and soft rocks were found to be dominated by arching, at least for friction angles beyond 20°. Once the friction angle is beyond this value, stability appears to be independent of the ground cover as well as possible surface loads. For shield tunnelling, this leads to an extremely simple expression for the minimum support pressure required. For open face tunnelling, it results in rules for the maximum diameter of the excavation and it involves the cutting-length. Considering small cutting lengths, the very simple approximate stability criteria of $\gamma D < 10\ c'$ was found to apply. The diameter D may either be the full tunnel diameter or a subsection diameter of a sequential excavation. Instead of considering a maximum diameter, it is also possible to calculate a factor of safety for a fixed given value of the diameter.

In the last part of this study non-circular tunnels have been considered. In such cases an equivalent diameter, for use in the stability criteria, can be computed from the excavation area considered. Unfortunately the stability equations do not hold when the tunnel face is dominated by different ground layers. In such cases it is advocated to apply a non-linear finite element analysis and to use the so-called φ-c-reduction method. Even in the general case of layered ground the formulas for non-layered ground remain of interest for understanding tendencies and for validating different numerical models and computer codes.

In classical literature on the NATM one finds the concept of the mobilisation of a supporting ground ring around tunnels as a function of deformations. It would seem that we detected such a ring numerically quite directly. It is nicely visualised by plotting contours of deviatoric stresses $|\sigma_1 - \sigma_3|$. For circular tunnels such a ground ring is found to be elliptical.

It should be realised that not all aspects of tunnel heading stability have been addressed, e.g. not the destabilising effect of pore water pressure. When driving a shield tunnel under the ground-water table and drained conditions apply, the effective failure pressure naturally has to be increased by the pore water pressure. Moreover, one would have to use the submerged weight

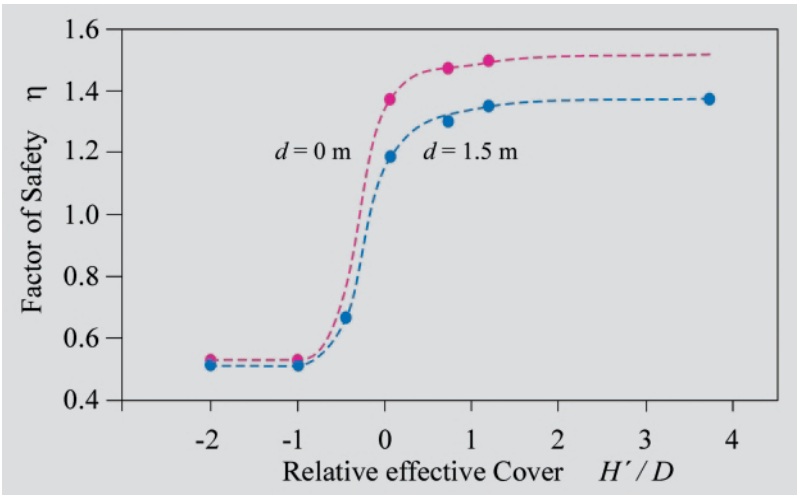

Fig. 15 Factor of safety as a function of the effective cover.

Bild 15 *Der Standsicherheitsfaktor als Funktion der effektiven Tunnelüberdeckung.*

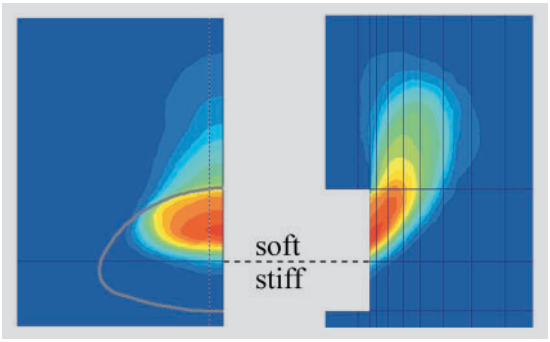

Fig. 16 Local failure inside the soft top layer for d = 0.

Bild 16 *Ein lokaler Verbruch bildet sich in der oberen Bodenschicht aus (für d = 0).*

γ' in all previous formulas. When open face tunnels are driven under the ground-water table and drained conditions apply, the water has an additional destabilising effect due to groundwater flow towards the tunnel heading, which has not been considered in this paper.

The present equations do not always apply to tunnelling in saturated clays, as they behave initially undrained with c_u as the undrained shear strength. For such situations, the equation $p_f = -c_u T_c + \sigma_0$ applies, where σ_0 is the initial vertical overburden stress at the tunnel axis. Atkinson and Mair (2) used model test data to derive design curves that give T_c as a function of H/D and d/D. For a standstill, however, drained conditions will occur and one may apply the formulas of the present study.

It should also be realised that perfect plasticity is a strong assumption, when considering highly cohesive clays and weak rocks that show a peak strength and a much lower residual strength. This softening with its resulting tendency of progressive failure is well-known for clay slopes, e.g. by the papers of Chen et al. (7) and Potts et al. (16), but as yet it was not thoroughly investigated for tunnel heading stability. For the two-dimensional problem of a fully unlined tunnel, consequences of softening are studied in another paper in the same issue of this journal. For the three-dimensional problem of a tunnel heading, it is a topic of further research.

Finally it should be realised that attention has been purely focused on stability and not on surface settlements, which are important for tunnelling in urban areas. There is no doubt that the successful design of tunnel excavations in such areas is based on both stability and deformation considerations.

References

1. Anagnostou, G. ; Kovári, K.: Face Stability Conditions with Earth-Pressure-Balanced Shields. In: *Tunnelling and Underground Space Technology* 11 (1996), No. 2, pp. 165-173.
2. Atkinson, J.H. ; Mair, R.J.: Soil mechanics aspects of soft ground tunnelling. In: *Ground Engineering* 14 (1981), No. 5, pp. 20-38.
3. Baumann, T. ; Sternath, R. ; Schwarz, J.: *Face stability of tunnels in soft rock – Possibilities for the computational analysis*. Proc. 14th Int. Conf. Soil Mech. Found. Engng, Hamburg, Vol. 3, pp. 1389-1392. Rotterdam: A.A. Balkema, 1997.
4. Brinkgreve, R.B.J. ; Bakker, H.L. : *Non-linear finite element analysis of safety factors*. Proc. 7th Int. Conf. Computer Methods and Advances in Geomechanics, Cairns, Vol. 2, pp. 1117-1122. Rotterdam: A.A. Balkema, 1991.
5. Brinkgreve, R.B.J. ; Vermeer, P.A.: *Manual of Plaxis 3D Tunnel*. Rotterdam: A.A. Balkema, 2001.
6. Chambon, J.F. ; Corté, J.F.: Shallow tunnels in cohesionless soil: Stability of tunnel face. In: *J. Geotech. Engng ASCE* 120 (1994), No. 7, pp. 1150-1163.
7. Chen, Z. ; Morgenstern, N.R. ; Chan, D.H.: Progressive failure of the Carsington Dam: a numerical study. In: *Can. Geotech. J.* 29 (1992), No. 6, pp. 971-988.
8. Davis, E.H. ; Gunn, M.J. ; Mair, R.J. ; Seneviratne, H.N.: The stability of shallow tunnels and underground openings in cohesive material. In: *Géotechnique* 30 (1980), No. 4, pp. 397-416.
9. Dawson, E.M. ; Roth, W.H. ; Drescher, A.: Slope stability analysis by strength reduction. In: *Géotechnique* 49 (1999), No. 6, pp. 835-840.
10. Itasca Consulting Group Inc.: *FLAC Version 4.0. User´s Guide*. Itasca consulting Group Inc., Minneapolis, 2002.
11. Jancsecz, S. ; Steiner, W.: *Face support for large mix-shield in heterogeneous ground conditions*. Proc. Tunnelling ´94, London, pp. 531-550. London: Chapman & Hall, 1994.
12. Kimura ; Mair (1981). Centrifugal Testing of Model Tunnels in Soft Clay. Proc. 10th Int. Conf. Soil Mech. Found. Engng, Stockholm, Vol. 1, 319-322. Rotterdam: A.A. Balkema Publishers.
13. Krause, T.: *Schildvortrieb mit flüssigkeits- und erdgestützter Ortsbrust*. Report of the Inst. of Geotech. Engng of the University of Braunschweig, Report No. 24, 1987.
14. Léca, E. ; Dormieux, L.: Upper and lower bound solutions for the face stability of shallow circular tunnels in frictional material. In: *Géotechnique* 40 (1990), No. 4, pp. 581-606.
15. Pacher, F.: *Deformationsmessungen im Versuchsstollen als Mittel zur Erforschung des Gebirgsverhaltens und zur Bemessung des Ausbaus*. Felsmechanik und Ingenieurgeologie, Supplementum I. Wien: Springer, 1964.
16. Potts, D.M. ; Kovacevic, N. ; Vaughan, P.R.: Delayed collapse of cut slopes in stiff clay. In: Géotechnique 47 (1997), No. 5, pp. 953-982.
17. Rabcewicz von, R.: *Gebirgsdruck und Tunnelbau*. Wien: Springer, 1944.
18. Semprich, S.: *Berechnung der Spannungen und Verformungen im Bereich der Ortsbrust von Tunnelbauwerken in Fels*. Report of the Inst. of Geotech. Engng of the RWTH Aachen, Report No. 8, 1980.
19. Sternath, R. ; Baumann, T.: *Face support for tunnels in loose ground*. World Tunnel Congress Wien´97. Rotterdam: A.A. Balkema, 1997.
20. Vermeer, P.A. ; Ruse, N.: Die Stabilität der Tunnelortsbrust in homogenem Baugrund. In: *geotechnik* 24 (2001), No. 3, pp. 186-193.
21. Vermeer, P.A. ; Ruse, N.: *Neue Entwicklungen in der Tunnelstatik*. Proc. 3rd Kolloquium Bauen in Boden und Fels, Technische Akademie Esslingen (ed.: Schad, H.), pp. 3-14. Ostfildern: TAE, 2002.
22. Vermeer, P.A. ; van Langen, H.: Soil collapse computations with finite elements. In: *Ingenieur-Archiv* 59 (1989),pp. 221-236.
23. Vermeer, P.A. ; Vogler, U.: On the stability of unlined tunnels. In Learned and Applied Soil Mechanics out of Delft (eds Barends & Steijger), pp. 127-134. Rotterdam: A.A. Balkema, 2002.
24. Zienkiewicz, O.C. ; Humpheson, C. ; Lewis, R.W.: Associated and non-associated visco-plasticity in soil mechanics. In: *Géotechnique* 25 (1975), No. 4, pp. 671-689.
25. Horn, M.: *Horizontaler Erddruck auf senkrechte Abschlußflächen von Tunnelröhren*. Landeskonferenz der Ungarischen Tiefbauindustrie, Budapest. Übersetzung ins Deutsche durch die STUVA, 1961.

Acknowledgements

The authors are indebted to Dr. ir. P. Bonnier from Plaxis for his support in the numerical calculations. The authors would also like to thank Dr.-Ing. habil. H. Schad for his very helpful comments and his thorough review of this paper.

Authors

Professor Dr.-Ing. Pieter A. Vermeer and Dipl.-Geol. Nico Ruse, Institute of Geotechnical Engineering, University of Stuttgart, Pfaffenwaldring 35, D-70569 Stuttgart, Germany, E-Mail vermeer@igs.uni-stuttgart.de; ruse@igs.uni-stuttgart.de, Dipl.-Ing. Thomas Marcher, ILF Consulting Engineers ZT GmbH, Framsweg 16, A-6020 Innsbruck, Austria, E-Mail thomas.marcher@ibk.ilf.com.